PERGAMON

International Journal of Heat and Mass Transfer 42 (1999) 1813–1833

International Journal of HEAT and MASS TRANSFER

The role of the Brinkman number in analysing flow transitions in microchannels

C.P. Tso*, S.P. Mahulikar

School of Mechanical and Production Engineering, Nanyang Technological University, Nanyang Avenue, Singapore 639798

Received 3 March 1998; in final form 3 August 1998

Abstract

The experimental data in the literature have indicated that there are unexplained unusual behaviours in heat transfer and flow in microchannels. In particular, the geometry of the microchannels and Reynolds number alone do not determine the flow regime boundaries and the transition range. The reported experimental data on convection in microchannels are now processed based on the correlation with the Brinkman number, from which the Reynolds and Brinkman numbers at the flow transition points are obtained for a fixed microchannel geometry. In addition to the Reynolds number, the Brinkman number is also discovered to determine the flow regime boundaries from laminar-to-transition and from transition-to-turbulent flow. The transition range varies due to the difference in the extent of the role played by the Brinkman number in determining the two flow regime boundaries.

Key words: Microchannel; Brinkman number; Flow transition; Forced convection

Nomenclature

a, b, c, d, e indices in equation (1.1)
Br Brinkman number of coolant in microchannel $\{=\mu \cdot V_m^2/k \cdot \Delta T\}$
c specific heat of coolant in the microchannel [J kg^{-1} K^{-1}]
C coefficient defined in equation (2.1)
D_h hydraulic diameter of microchannel [m]
f_i dimensionless function determining flow transitions in equation (1)
f_g dimensionless function of geometry of microchannels in equation (2)
h convective heat transfer coefficient in microchannel [W m^{-2} K^{-1}]
H height of microchannel [m]
k axially local and sectionally-averaged coolant thermal conductivity [W m^{-1} K^{-1}]
m exponent of Re in equation (2.1)
Nu Nusselt number in microchannel
Pr Prandtl number of coolant in microchannel
q''_w sectionally-averaged wall heat flux [W m^{-2}]
Re Reynolds number of coolant flow in microchannel
T_f axially local bulk mean coolant temperature [K]
$T_{f,in}$ coolant temperature at microchannel inlet [K]
T_w sectionally-averaged temperature of microchannel wall [K]
V_m sectionally-averaged coolant velocity in microchannel [m s^{-1}]
W width of microchannel [m]
W_t centre-to-centre distance between two consecutive microchannels [m].

Greek symbols

ΔT axially local wall-coolant temperature difference $\{=|T_w - T_f|\}$ [K]
μ dynamic viscosity of coolant in microchannel [N s^{-1} m^{-2}]
v kinematic viscosity of coolant in microchannel [m^2 s^{-1}]
ρ density of coolant in microchannel [kg m^{-3}].

Subscripts

tr value at transition point.

* Corresponding author. Tel.: 0065 790 5033; fax: 0065 791 1859; e-mail: mcptso@ntu.edu.sg

0017–9310/98/$ - see front matter
PII: S0017–9310(98)00276–2

1. Introduction

It has been reported that the heat transfer and flow behaviour in microchannels differs considerably from the conventionally-sized channels. Peng and Wang [1] in 1993 experimentally investigated the heat transfer characteristics of subcooled liquid flow through rectangular microchannels, and found that h was enhanced, confirming the early findings of Tuckermann and Pease [2], and that the velocity and subcooling may influence the single-phase convection. Peng et al. [3] experimentally investigated the flow characteristics of water flowing through rectangular microchannels having D_h in the range of 0.133–0.367 mm and (H/W) in the range of 0.333–1. Their measurements indicated that the upper bound of the laminar flow regime occurred in the Re range of 200–700, and fully turbulent flow was reached in the Re range of 400–1500. The critical Re for the laminar transition was found to be strongly affected by D_h, decreasing with corresponding decreases in D_h. In addition, the size of the transition range was found to diminish, and fully turbulent flow was found to occur at a much lower Re. The geometric parameters, D_h and H/W, were found to affect the flow strongly. In another paper [4], they reported their experimental investigation of forced convective heat transfer of water flow in rectangular microchannels having D_h in the range of 0.133–0.367 mm and (H/W) in the range of 0.333–1, and reported that Nu is proportional to $Re^{0.62}$ in the laminar regime. They measured the flow friction to analyse the heat transfer regimes and to explore the physical aspects of convection, and revealed that the same geometric parameters reported in [3] had significant influence on the convective heat transfer and flow transition characteristics.

Wang and Peng [5] investigated the influence of liquid flow, thermal parameters, geometrical size and structure on the single-phase forced convection characteristics, for the flow of methanol and deionized water through microchannels with rectangular cross-section. The behaviour of h was found to be highly associated with the liquid flow or the heat transfer mode, which implies that there exists separate heat transfer mechanisms accordingly, which were then unexplained. For Re values greater than about 1500, all data taken from their different test sections fell close to a single straight line on the log–log graph, which represents the turbulent flow. For $700 < Re < 1500$, some data also fell along the same line, while some data fell above the line. This implies that fully turbulent flow does not occur at a fixed Re. For $Re < 700$, the relationship between Nu and Re was found to be complex. When transition appeared, Nu was found to be almost independent of Re for a specified V_m and $T_{f,in}$, since the convective heat transfer coefficient h was found to be independent of the wall temperature T_w. Prior to the transition zone, Nu was found to recede with increasing Re, which is the laminar flow zone. Hence the transition and laminar convection were reported to be strange compared with the conventionally-sized situations. By decreasing V_m and increasing $T_{f,in}$, the transition to turbulent flow was found to occur at a lower Re and the transition zone in which Nu is nearly constant was found to be enlarged. Hence, the transition point and range, and the convective heat transfer characteristics of transition and laminar flows were found to be affected by $T_{f,in}$, V_m, and microchannel size. All these phenomena were observed at a lower Re as the microchannel size became smaller for a specified V_m and $T_{f,in}$. Hence the role of convective heat transfer in flow transitions is explicit, since the convective heat transfer characteristics reflect the flow mode.

Peng et al. [6] reported the investigation on the cooling performance of methanol flow through rectangular microchannels. They have presented their experimental results of heat flux $\dot{q}''_w$ and h with respect to T_w, for various channel geometries, V_m and $T_{f,in}$, which show a rapid rise in h at low values of T_w, indicating a transition of the liquid flow regime. The V_m was found to have a significant influence on the flow mode, since changes in V_m significantly altered the profiles of $\dot{q}''_w$ or h versus T_w curves, resulting in transitions from laminar to transition flow and from transition to turbulent flow. They also found the existence of a flow mode transition region, beyond which h is nearly independent of T_w. These transitions were also found to be a function of the T_w conditions within the microchannels, and to be a direct result of the large T_f rise, causing significant liquid property variations and increase in the relevant flow parameters, such as the Reynolds number. The flow transition was found to occur at lower values of T_w when V_m was higher. Hence, the liquid velocity and subcooling were concluded to be instrumental in determining the point or region where the transition occurs, thereby supporting the findings reported in [5]. However they did not explain the dependence of the transition point and range on these parameters. The transitions were also found to depend on the size and number of microchannels, thereby supporting the dependence on geometry, reported in [3–5].

Peng and Peterson [7] have conducted experiments for water flow with different microchannels, to determine the influence of liquid flow, thermal conditions and microchannel size on the flow and forced convective heat transfer characteristics. Their results proved the existence of three distinct flow regimes, and indicated that laminar flow exists for $Re < 400$, a transition regime in the region of $300 < Re < 1000$, and a turbulent regime for $Re > 1000$. The flow transitions and transition range were found to be influenced by $T_{f,in}$ and V_m as mentioned in [5, 6], and on microchannel size as reported in [3–6]. In another paper [8]. they have compared their correlations between Nu, Re, Pr and a dimensionless geometric parameter of the microchannels with their experimental data,

for the laminar and turbulent regimes. They have presented the laminar regime correlation for *Re* range 70–1000, and the turbulent regime correlation for *Re* range 400–4000. However in the *Re* range of 70–1000, the experimental data points do not seem to significantly deviate from the laminar regime correlation, suggesting that the *Re* exponent of 0.62 in their laminar regime correlation, may not be sensitive to flow regime change from laminar to transition. Hence *Re* alone may not be significant in determining the flow transition, especially from laminar to transition flow.

Recently, Tso and Mahulikar [9] have shown *Br* to correlate the forced convective heat transfer in the laminar and transition regimes, and hence explained the unusual behaviour of convective heat transfer in microchannels. This paper extends the findings reported in [9] to analyse the unusual behaviour associated with the flow transitions. As reported in [5–7], apart from the geometric parameters of the microchannel, V, ΔT and variations in μ, affect the flow transitions and the transition range, and these parameters are incorporated in *Br*, which suggests that *Br* plays a role in determining the flow transitions and the transition range. Since the survey indicated that the flow mode is reflected in the heat transfer characteristics, the correlation with *Br* is plotted from which the flow modes are extracted. As the laminar-to-transition and transition-to-turbulence boundaries identify the transition range, the values of *Re* and *Br* are noted at these changes and their loci plotted to obtain the range. Since the literature indicates a variable transition range bounded by these transitions, the loci of these transitions are plotted on the *Br* versus *Re* graph.

2. Processing of reported experimental data

Only the experimental data presented by Wang and Peng [5] can be further processed to obtain *Br* and hence the correlations including *Br*, as mentioned in [9]. They have presented their experimental data of h with T_w [in their Fig. 3(a)–(f)] and of *Nu* with *Re* [in their Fig. 6(a)–(d)] for the six different microchannel geometries (test section nos. 1–6). For each geometry, the variation presented is for a fixed V_m and $T_{f,in}$. Since they have not given the variation of *Nu* with *Re* for their test section no. 1, the data for no. 1 cannot be further processed. The data for the other 5 geometries, totalling 356 points, are processed. Most of the data points in their Figs 3 and 6 for each geometry exhibit a one-to-one correspondence, which has been confirmed by comparing the calculated *Nu* from the h value given in Fig. 3, with the *Nu* given in Fig. 6. However, for some data sets, the number of data points in their Figs 3 and 6 do not match, in which case the one-to-one correspondence between the individual data points is obtained by matching the calculated *Nu* from the h given in Fig. 3, with the *Nu* given in Fig. 6. The laminar data, of their test section no. 6, for $V_m = 0.25$ m s^{-1} and $T_{f,in} = 19.7$°C, $V_m = 0.29$ m s^{-1} and $T_{f,in} = 18.8$°C, $V_m = 0.76$ m s^{-1} and $T_{f,in} = 19.3$°C, are also in [9]. The procedure for data processing to obtain all the required parameters is the same as described in [9].

3. Observation and analysis of processed data

3.1. Observation of processed experimental data

Figure 1(a)–(e) shows the plot of the parameter $Nu \cdot [Re^{0.62} \cdot Pr^{1/3}]^{-1}$ versus *Br* for test section nos. 2–6. The *Br* reduces along the flow due to decrease in the dynamic viscosity μ of the coolant and increase in the ΔT.

As a illustration, Figs 2(a) and (b) compares the typical trends of *Nu* versus *Re*, and $Nu \cdot [Re^{0.62} \cdot Pr^{1/3}]^{-1}$ versus Br^{-1} respectively. The reciprocal of *Br* is plotted in fig. 2(b) to bring about the same direction of flow along the abscissa, as is the case with increasing *Re* in Fig. 2(a). The laminar regime here is represented by data from test section no. 6, the transition regime is represented by most of the data from test section no. 4, and the turbulent regime is represented by data from test section no. 2. The flow is fully turbulent when the parameter follows a constant trend, which is exhibited by the limited data available in the fully turbulent regime. From Fig. 2(b), it is seen that in the laminar regime, the parameter $Nu \cdot [Re^{0.62} \cdot Pr^{1/3}]^{-1}$ reduces as Br^{-1} increases. The turning point, where the gradient changes sign corresponds to the change from laminar to transition (marked 'A' in Fig. 2(b)). Thereafter, the parameter increases and again decreases as Br^{-1} increases, and the region in which the parameter increases and then decreases, covers the transition regime. The region where the parameter increases as Br^{-1} increases may be classified as the low transition region and the region where the parameter reduces as Br^{-1} increases may be classified as the high transition region. The point 'A' can also be identified in Fig. 2(a).

For the transition to turbulent point, it is much easier to identify it in Fig. 2(b) than in Fig. 2(a). In the plot of *Nu* versus *Re*, *Nu* is approximately independent of *Re* after the laminar regime, and in the turbulent regime the modified Dittus–Boelter is obeyed [4, 5, 8]. Hence in the fully turbulent regime, the plot of $Nu \cdot [Re^{0.8} \cdot Pr^{1/3}]^{-1}$ versus Br^{-1} for a given microchannel geometry would be almost horizontal whereas the plot of $Nu \cdot [Re^{0.62} \cdot Pr^{1/3}]^{-1}$ versus Br^{-1} increases monotonically. Thus it is seen that in the plot of *Nu* versus *Re*, the slope of the graph in the transition and turbulent regimes changes in magnitude but not in sign, whereas in the graph of $Nu \cdot [Re^{0.62} \cdot Pr^{1/3}]^{-1}$ versus Br^{-1}, the slope changes its sign. Hence, the turning point in the plot of $Nu \cdot [Re^{0.62} \cdot Pr^{1/3}]^{-1}$ versus Br^{-1} gives a clearer indication of the flow mode and its

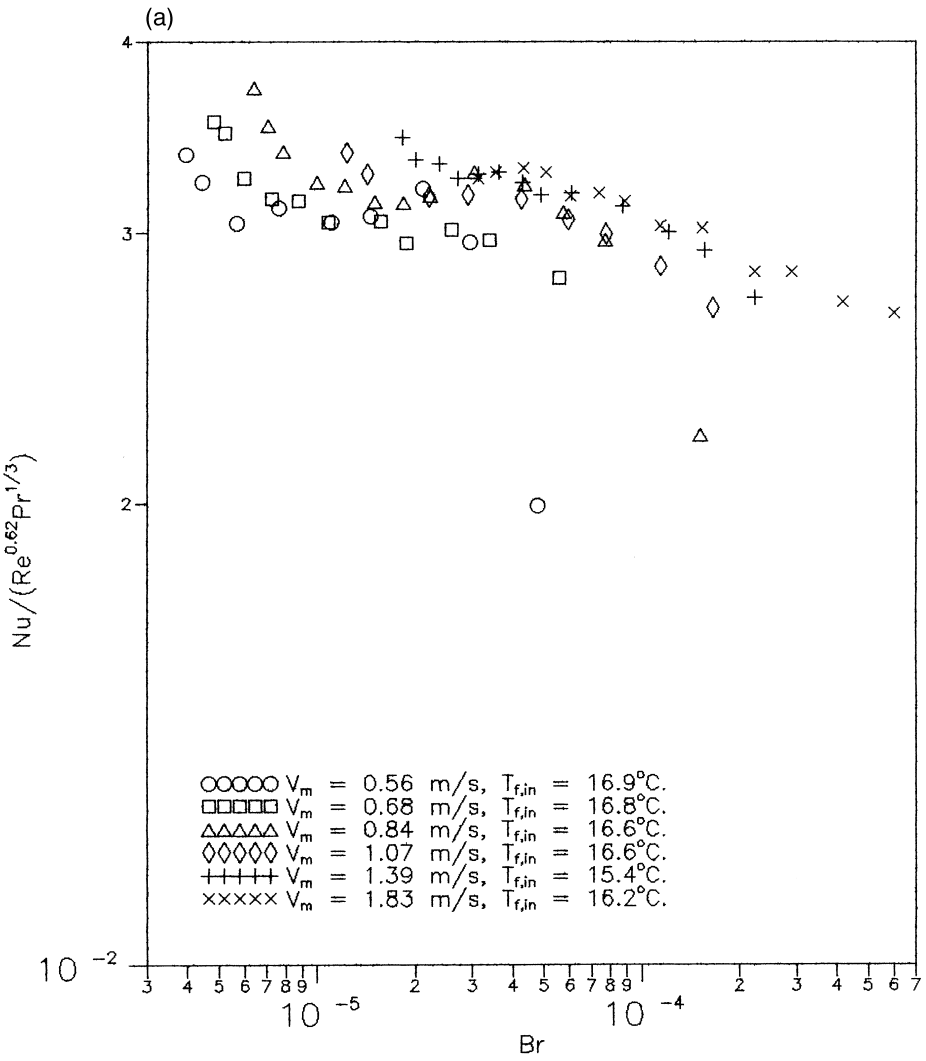

Fig. 1. Plot of $Nu \cdot [Re^{0.62} \cdot Pr^{1/3}]^{-1}$ versus Br. (a) test section no. 2; (b) test section no. 3; (c) test section no. 4; (d) test section no. 5; (e) test section no. 6.

transition. This is observed by comparing Fig 2(a) and (b) (point 'B' indicates change from transition to turbulent).

In the plot of Nu versus Re, Nu is nearly constant in the transition regime, but in the plot of $Nu \cdot [Re^{0.62} \cdot Pr^{1/3}]^{-1}$ versus Br^{-1}, the parameter increases and then decreases as Br reduces, for reasons mentioned in [9]. When the parameter further increases as Br further reduces, the flow enters the turbulent mode.

The above trends are observed universally in Fig. 1, and based on the observation of these trends, the flow regimes for the various cases are identified and presented in Table 1. The Re and Br values at the transition points are noted.

Since the exponent of Re in the convective heat transfer correlation is reported to be 0.62 in the laminar regime [4, 8] and 0.8 in the turbulent regime [4, 5, 8], the transition regime is expected to have an exponent between 0.62 and 0.8. However from the present study, the Re values at the flow transition points do not change. Hence, the variations in Fig. 1 are adequate for obtaining the flow transition points. This is seen by plotting the parameter $Nu \cdot [Re^{0.8} \cdot Pr^{1/3}]^{-1}$ versus Br for test section no. 2 in Fig. 3, as an illustration. Comparing Figs 1(a) and 3, it is seen that the parameter in Fig. 3 takes a lower value than in Fig. 1(a) due to higher value of the Re exponent. However, the qualitative trend is the same, and the Br values at which the trends change are not altered (indicated by vertical arrows in Fig. 3).

Though the number of experimental data points processed to obtain the single-phase convective heat transfer

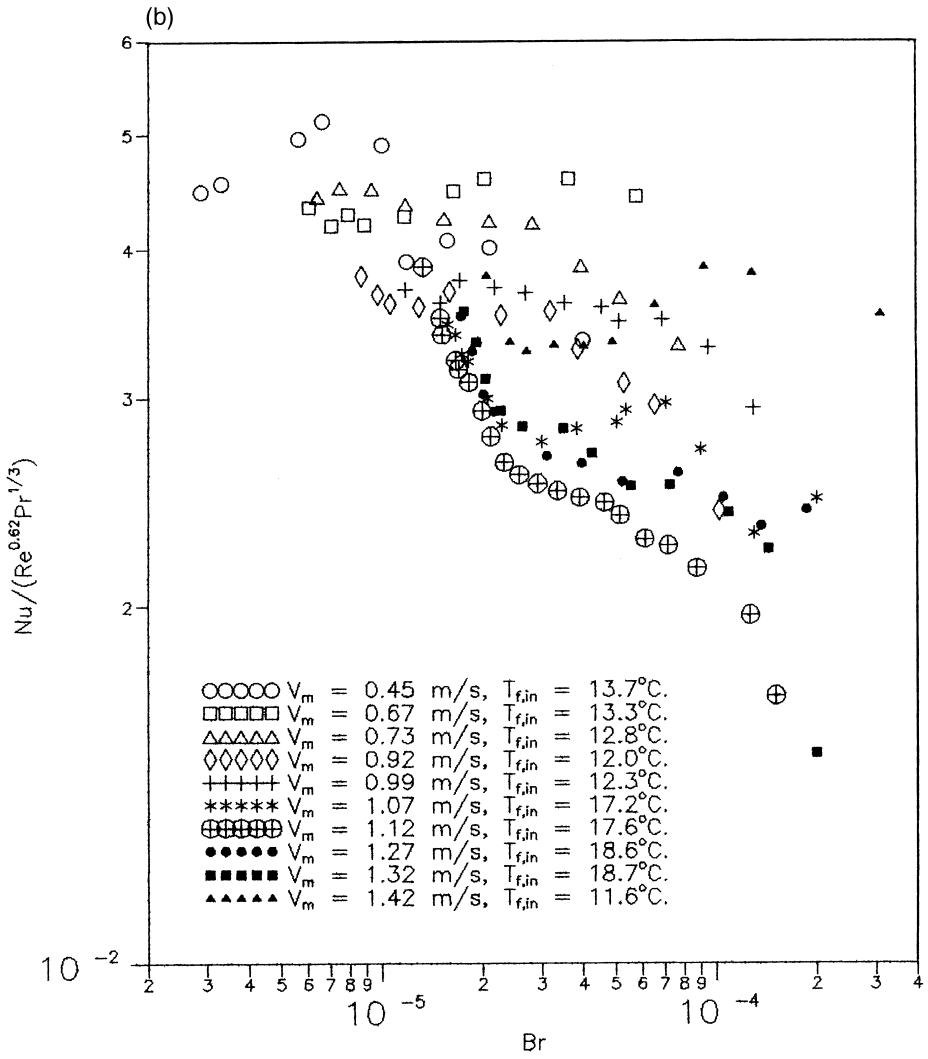

Fig. 1—*continued.*

correlation for a given velocity and geometry may be large, only one flow transition point can be obtained for a given microchannel geometry and a given velocity, and that too only if there is more than one flow mode.

3.2. Proposed form of correlation

A form for correlating the flow transition points for obtaining the flow regime boundaries is proposed, based on dimensional analysis. Since it is known for the conventionally-sized channels that Re alone determines the flow regime boundary, the criterion for flow transitions is of the form Re_{tr} = constant, and hence Re is also expected to play a role in microchannels. Hence the parameters ρ, V_m, D_h and μ, play a role in flow transitions in microchannels. Furthermore, since the literature indicates that ΔT affects the flow transitions, k and ΔT should also be pertinent parameters for consideration, since the role of ΔT is to cause heat flow by conduction across the slow moving fluid boundary layer. Since the amount of heat transferred by conduction depends upon the resistance of the fluid and the spacing between microchannels, H, W and W_t, may also play a role in flow transitions. Hence a general criterion determining the flow regime boundaries is given as

$$f_1(\rho, V_m, D_h, \mu, k, \Delta T, H, W, W_t) = \text{constant}, \quad (1)$$

where f_1 is a dimensionless unknown function to be found. In [9], h and c have been used in addition in the dimensional analysis, since the purpose of the dimensional analysis there was to obtain a correlation for h, and literature indicated that h also depends on c. However,

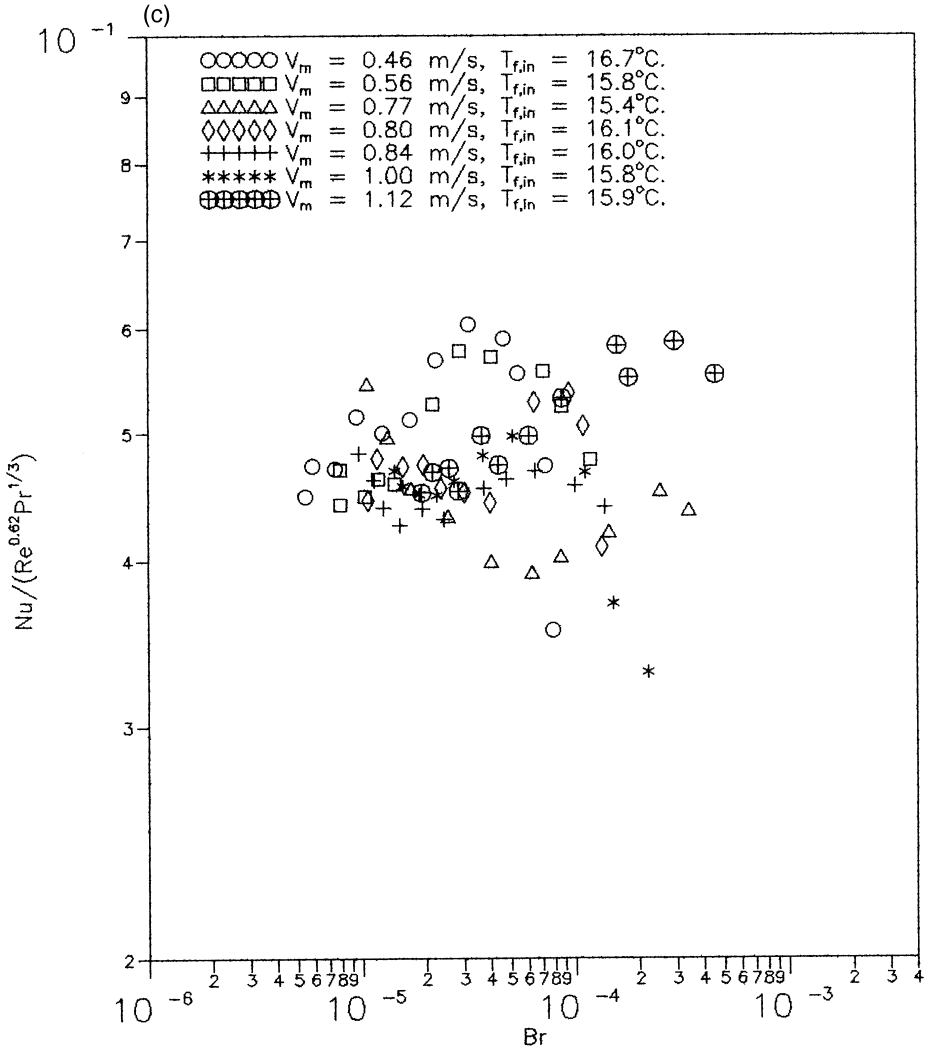

Fig. 1—*continued.*

in the present study, the objective is to obtain a parameter determining the flow regime boundaries, hence the function f_1 is equated to a constant at the boundaries. Using a similar procedure for the dimensional analysis as in [9], the five dimensionless groups obtained are W/D_h, H/D_h, W_t/D_h, Re and Br. Hence a general correlation may be written in the form

$$(Re_{tr})^a \cdot (Br_{tr})^b \cdot (W/D_h)^c \cdot (H/D_h)^d \cdot (W_t/D_h)^e = \text{constant}, \tag{1.1}$$

where a, b, c, d, and e are the indices. Equation (1.1) may be re-written as

$$(Re_{tr})^{\frac{a}{b}} \cdot (Br_{tr}) \cdot (W/D_h)^{\frac{c}{b}} \cdot (H/D_h)^{\frac{d}{b}} \cdot (W_t/D_h)^{\frac{e}{b}} = \text{constant}, \tag{1.2}$$

which may be rewritten as

$$\frac{Re_{tr}^m}{Br_{tr}} \cdot f_g(H, W, W_t, D_h) = \text{constant}, \tag{2}$$

where f_g is a dimensionless geometric function of the individual microchannels and the structure of microchannels. Hence if the microchannel geometry is fixed, equation (2) reduces to

$$Br_{tr} = C \cdot Re_{tr}^m. \tag{2.1}$$

3.3. Loci of laminar-to-transition and transition-to-turbulent boundaries

The loci of transition-to-turbulent boundary for test section nos. 2 and 3 are plotted in Fig. 4(a), and the loci

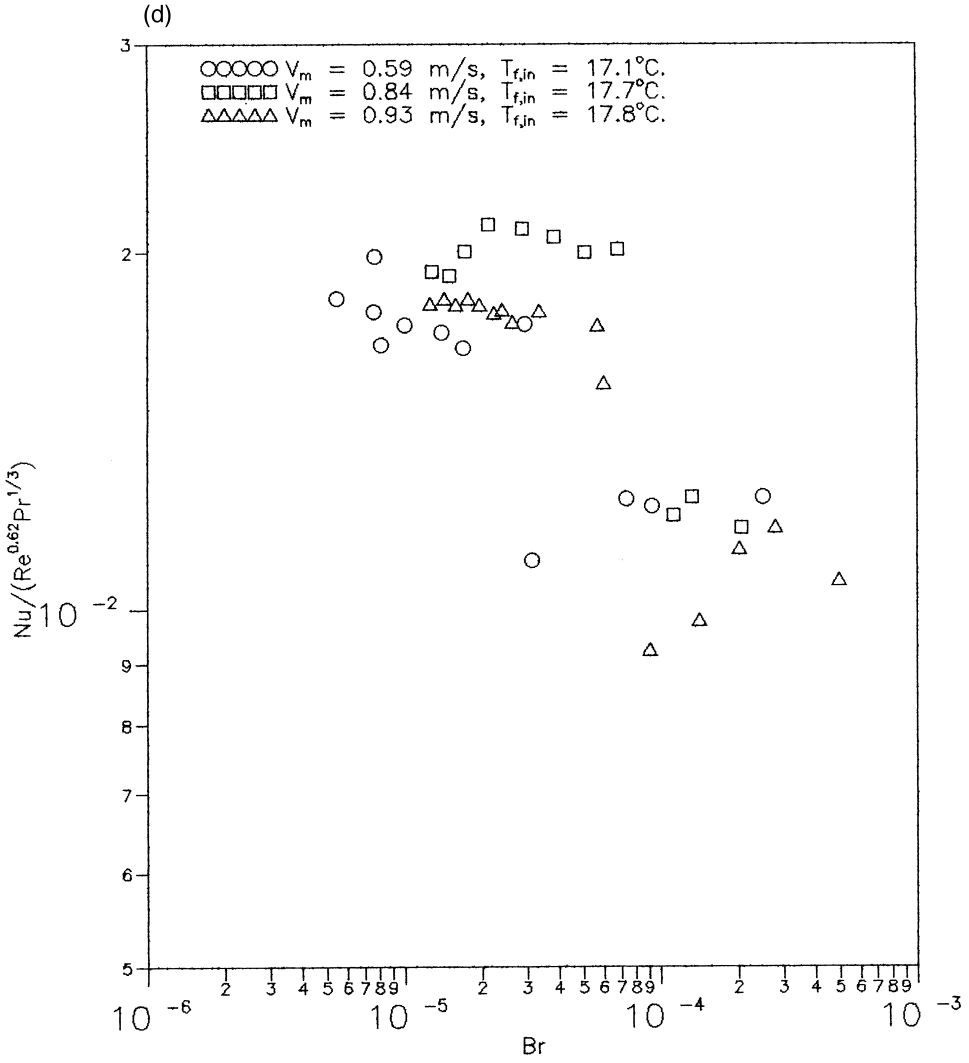

Fig. 1—*continued.*

of laminar-to-transition boundary for test section nos. 5 and 6 are plotted in Fig. 4(b). The values of the exponent m and coefficient C in equation (2.1) and their standard deviations are also given in Table 1. From these graphs the role of Br in determining flow transitions for a given microchannel geometry is evident, because if the flow transitions depend purely on Re, its exponent m in equation (2.1) would be infinity. If $|m| > 1$, the role of Re in determining flow transitions is higher than the role of Br, and as m increases, the role of Br drops further. The positive values of m imply that as Br_{tr} reduces, the transition occurs at a lower Re. This accounts for the observation in [5] that by decreasing V_m and increasing $T_{f,in}$, the transition to turbulent flow occurs at a lower Re, since decreasing V_m reduces Br_{tr}, and to keep the ratio Re_{tr}^m/Br_{tr} where $(m > 3)$ constant, Re_{tr} must reduce. The correlation of the transition with Br also supports the observation reported in [6] that transition occurs at a lower T_w when V_m is higher. Assuming that the density ρ and the thermal conductivity k of the coolant do not significantly change with T_f, equation (2.1) simplifies to

$$\frac{V_m^{m-2}\cdot(T_w - T_f)}{\mu^{m+1}} = \text{constant}. \tag{3}$$

From equation (3) it is seen that for low values of T_w the values of T_f are also low, and hence the wall-coolant temperature difference ΔT is small. However μ^{m+1} is large at low values of T_f, hence the ratio $\Delta T/\mu^{m+1}$ is small at low values of T_f. Hence from equation (3), V_m must increase.

It is easier to identify the laminar-to-transition bound-

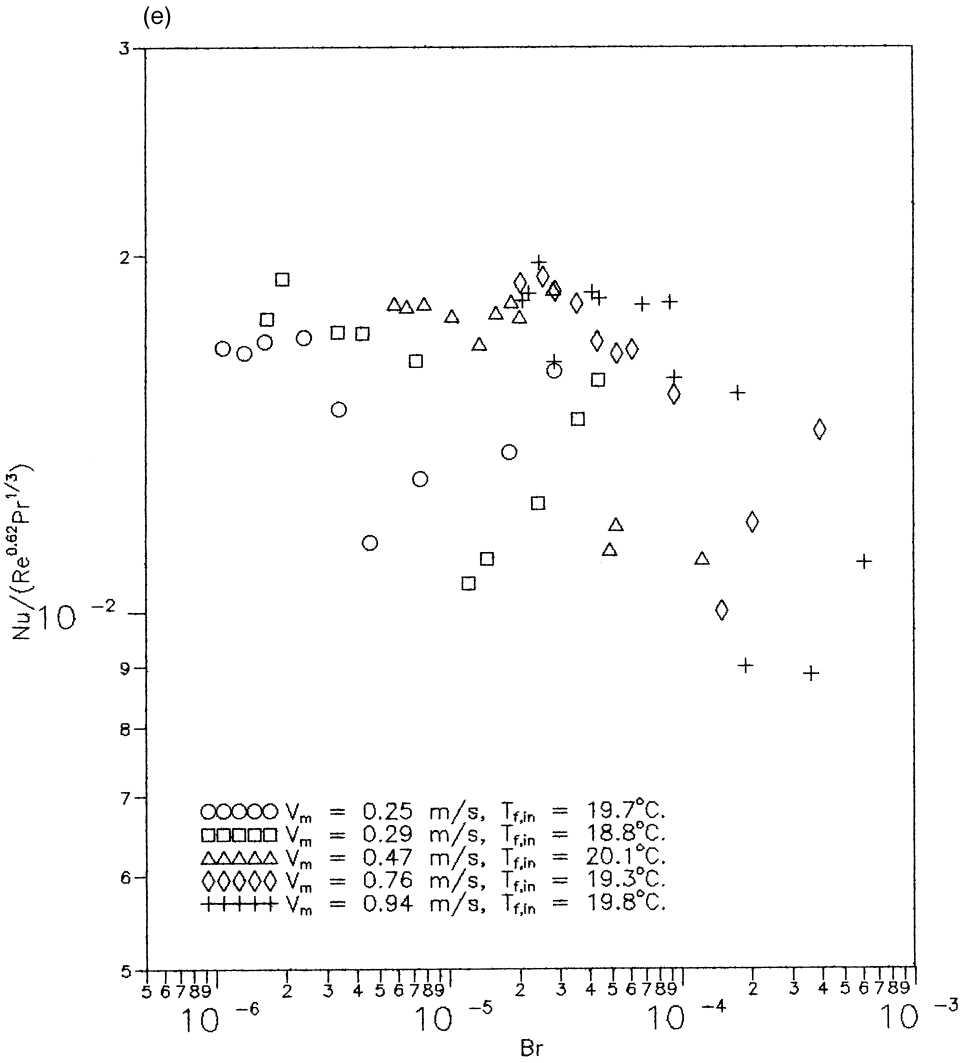

Fig. 1—*continued.*

ary than the transition-to-turbulent boundary, since in the latter case the transition flow changes to fully turbulent flow gradually after the onset of turbulence. Furthermore, at high transition values of Re, a small error in locating Br_{tr} results in a relatively large error in Re_{tr}, thereby increasing the error in locating the transition-to-turbulent boundary. Hence, the differences in the values of m and C are higher for the transition-to-turbulent boundary (test section nos 2 and 3) than for the laminar-to-transition boundary (test section nos 5 and 6). The H and W for test sections 5 and 6 are the same, but the value of W_t is different. However, this difference is not expected to significantly alter the exponent m, though the coefficient C may vary due to variation in the dimensionless geometric function f_g. Hence a typical laminar-to-transition boundary for the microchannel geometries studied may be represented by the form

$$Br_{tr} = C \cdot Re_{tr}^{3.4}. \tag{4}$$

3.4. Variation of transition range

Comparing the exponent m for the transitions, it seen that the value of m for the laminar-to-transition boundary is always lower than for the transition-to-turbulent boundary. This conclusion holds in spite of the uncertainty in identifying the transition-to-turbulent boundary. Hence, Br has a relatively greater role in determining the laminar-to-transition boundary, than the transition-to-turbulent boundary, i.e., the transition-to-turbulent

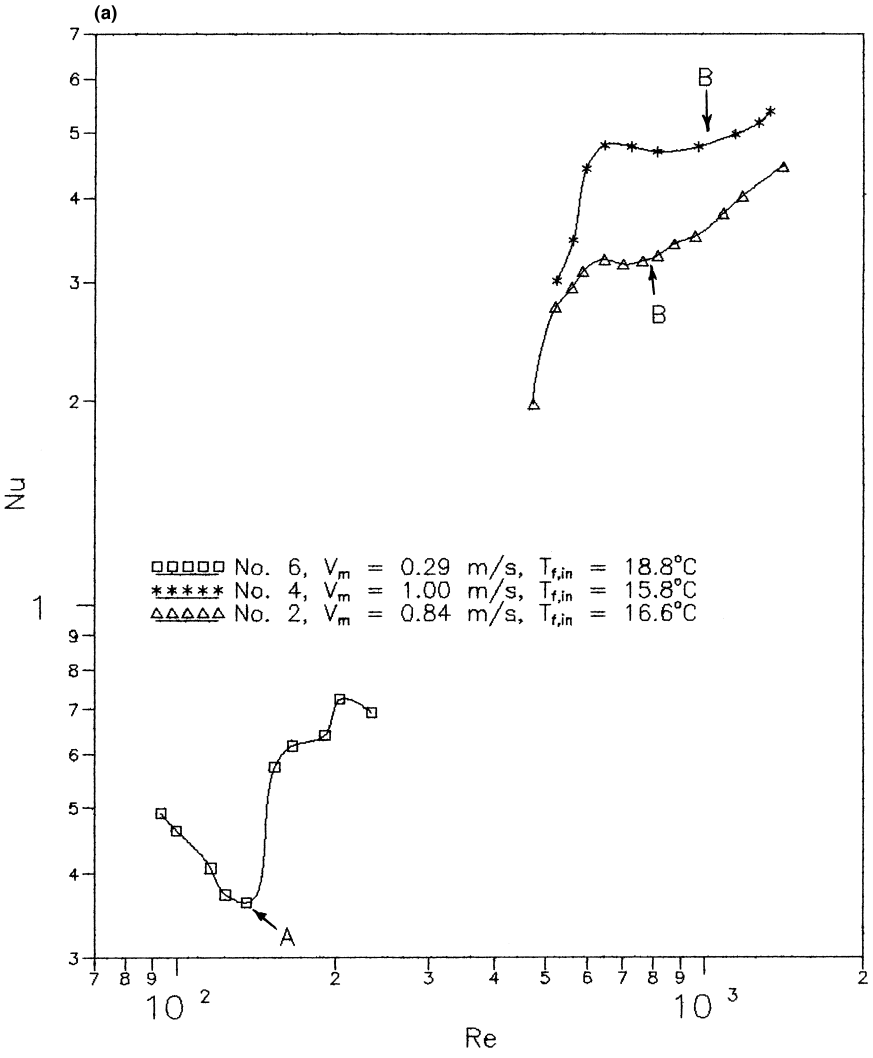

Fig. 2. Typical plot for test section nos. 2, 4 and 6; (a) plot of Nu versus Re; (b) plot of $Nu \cdot [Re^{0.62} \cdot Pr^{1/3}]^{-1}$ versus Br^{-1}.

boundary is relatively independent of Br. This is probably because Br in microchannels represents the ratio of velocity and temperature gradients as discussed in [9], and these gradients are well-maintained in the laminar regime, and in the high transition regime these gradients are poorly maintained, thereby reducing the significance of Br. Representative loci are obtained for the transition-to-turbulent boundary from test section nos 2 and 3, and for the laminar-to-transition boundary from the test section nos 5 and 6, by obtaining an average best-fit covering the range of Re and Br. These representative loci are shown in Fig. 5, which indicates the varying transition range. The representative loci for the laminar-to-transition boundary for the microchannel geometries studied is given by

$$Br_{tr} = 3.09 \times 10^{-13} \cdot Re_{tr}^{3.4}, \tag{5}$$

which may be written as

$$[Re_{tr}^{3.4}/Br_{tr}] = 3.24 \times 10^{12}, \tag{5.1}$$

and for the transition-to-turbulent boundary is given by

$$Br_{tr} = 2.96 \times 10^{-43} \cdot Re_{tr}^{13.2}, \tag{6}$$

which may be written as

$$[Re_{tr}^{13.2}/Br_{tr}] = 3.38 \times 10^{42}. \tag{6.1}$$

The laminar flow regime is given by $[Re^{3.4}/Br] < 3.24 \times 10^{12}$, the transition by $[Re^{3.4}/Br] > 3.24 \times 10^{12}$ and

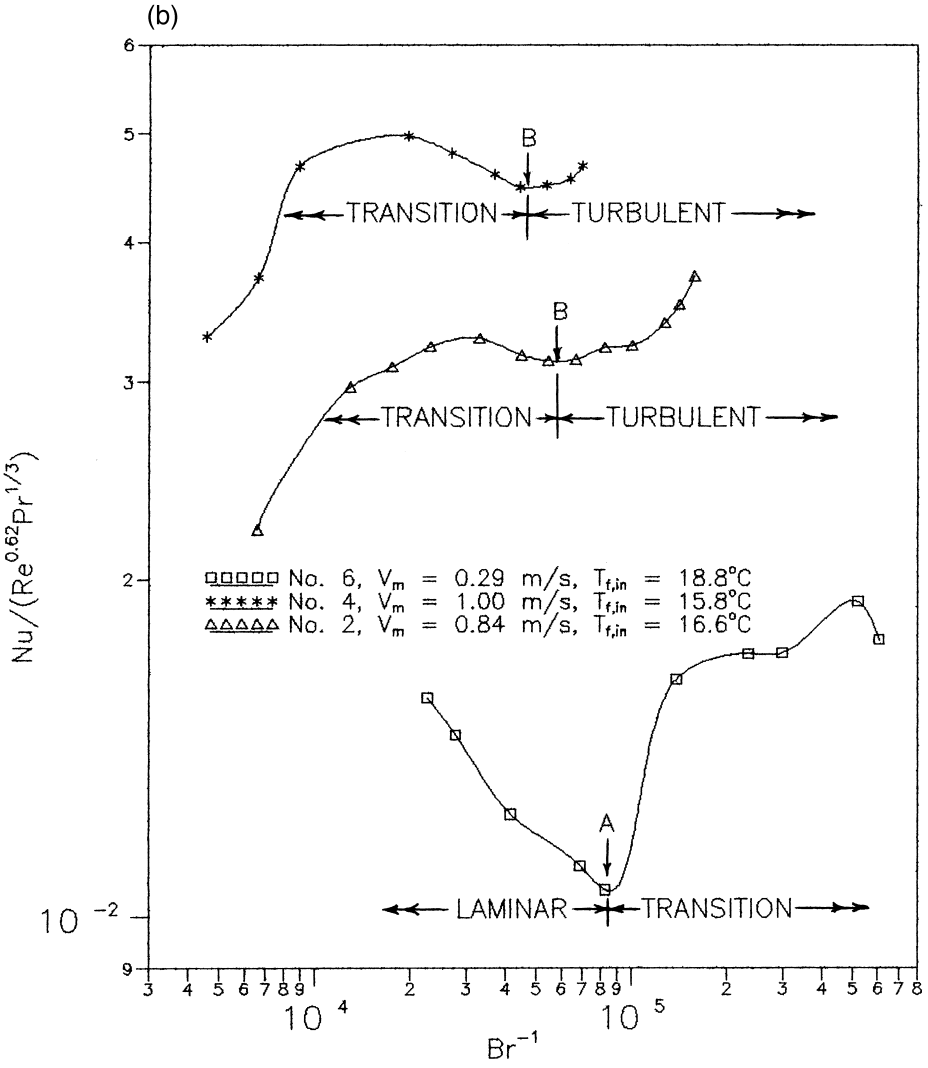

Fig. 2—*continued.*

$[Re^{13.2}/Br] < 3.38 \times 10^{42}$, and the turbulent by $[Re^{13.2}/Br] > 3.38 \times 10^{42}$.

Though the two transition loci should be obtained for the same geometry, the qualitative variation of the transition range indicated in Fig. 5 will not alter, since *Br* has a lesser role in determining the transition-to-turbulent boundary than in determining the laminar-to-transition boundary, even when the geometry is fixed. The representative loci for the flow regime boundaries are plotted on the loci of *Br* versus *Re* for a given V_m and $T_{f,in}$ in Fig. 6 (a)–(e) for the different test sections in [5], which shows the varying transition range as mentioned in [5–7]. As seen from these figures, the transition range is higher for smaller values of V_m as observed in [5]. Hence to obtain the complete flow range from laminar to transition flow over a short length of the microchannel, the V_m should be large.

3.5. *Plausible explanation for role of* Br

A plausible explanation for the role of *Br* in determining the flow regime boundaries may be attributed to the steep gradient of μ over the cross-section and along the flow, which causes a coupling between the momentum and energy equations at the differential level. In microchannels, the variation of μ over the cross-section also creates a significant shear stress gradient across the cross-section, in addition to the shear stress gradient created due to variation of the velocity gradient. By considering the free body diagram of an elemental fluid particle, it

Table 1
Flow modes identified from heat transfer characteristics of processed experimental data

Test section	V_m (m s^{-1}), $T_{f,in}$ (°C)	Flow modes	Re_{tr}, Br_{tr}
2	0.56, 16.9	Transition and turbulent	816, 4.4098×10^{-6}
(Fig. 4(a))	0.68, 16.8	Transition and turbulent	858, 7.2714×10^{-6}
	0.84, 16.6	Transition and turbulent	876, 1.2139×10^{-6}
	1.07, 16.6	Transition and turbulent	935, 4.2323×10^{-5}
	1.39, 15.4	Turbulent only	—
	1.83, 16.2	Turbulent only	—
	$m = 16.9\pm1.4$, $\log_{10}(C) = -54.8\pm4.1$		
3	0.45, 13.7	Transition only	—
(Fig. 4(a))	0.67, 13.3	Transition only	—
	0.73, 12.8	Transition only	—
	0.92, 12.0	Transition and turbulent	1055, 9.6884×10^{-6}
	0.99, 12.3	Transition and turbulent	1083, 1.1735×10^{-5}
	1.07, 17.2	Transition and turbulent	1122, 1.5634×10^{-5}
	1.12, 17.6	Transition and turbulent	1144, 1.6898×10^{-5}
	1.27, 18.6	Transition and turbulent	1152, 3.1813×10^{-5}
	1.32, 18.7	Turbulent only	—
	1.42, 11.6	Turbulent only	—
	$m = 10.8\pm2.5$, $\log_{10}(C) = -37.7\pm7.6$		
4	0.46, 16.7	Transition only	—
	0.56, 15.8	Transition only	—
	0.77, 15.4	Transition only	—
	0.80, 16.1	Transition only	—
	0.84, 16.0	Transition only	—
	1.00, 15.8	Transition only	—
	1.12, 15.9	Transition only	—
5	0.59, 17.1	Laminar and transition	239, 3.0490×10^{-5}
(Fig. 4(b))	0.84, 17.7	Laminar and transition	335, 9.0253×10^{-5}
	0.93, 17.8	Laminar and transition	378, 1.4163×10^{-4}
	$m = 3.32\pm0.06$, $\log_{10}(C) = -12.4\pm0.2$		
6	0.25, 19.7	Laminar and transition	115, 3.8822×10^{-6}
(Fig. 4(b))	0.29, 18.8	Laminar and transition	144, 9.0421×10^{-6}
	0.47, 20.1	Laminar and transition	206, 3.5772×10^{-5}
	0.76, 19.3	Laminar and transition	310, 1.1466×10^{-4}
	0.94, 19.8	Laminar and transition	373, 2.4633×10^{-4}
	$m = 3.47\pm0.09$, $\log_{10}(C) = -12.5\pm0.2$		

can be seen that shear forces acting on the two faces of the elemental fluid particle in opposite directions create a torque, which may induce rotational motion. The rotation may cause a cross-flow instability, which is the fundamental cause of turbulence. The ΔT in the term $(k\cdot\Delta T)$ in Br represents the gradient of μ across the cross-section due to the dependence of μ on the fluid temperature. The fact that Br in microchannels represents the ratio of velocity and temperature gradients, is elaborated in [9]. The $(\mu\cdot V_m^2)$ term is the average momentum transfer across the cross section, and its variation along the flow may also create instabilities. Hence, Br may also be a ratio of instabilities along the flow to instabilities across the flow in microchannels. In the conventionally-sized channels, the gradient of μ across the cross-section is generally small, since the fluid temperature gradient across the cross-section is small. Also because the mass flow rates are generally much larger, the variation of μ along the flow is negligible, and hence Br does not play a significant role in determining flow transitions.

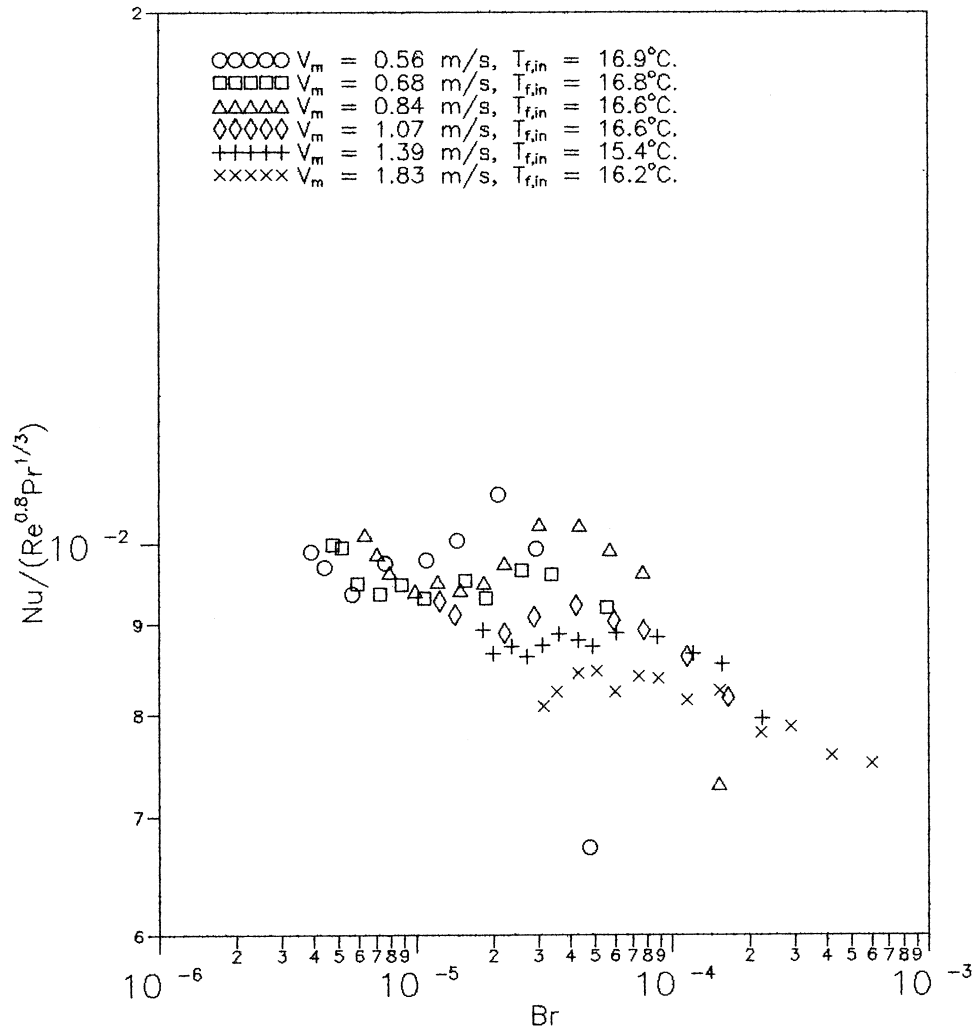

Fig. 3. Plot of $Nu \cdot [Re^{0.8} \cdot Pr^{1/3}]^{-1}$ versus Br for test section no. 2.

3.6. Scope for future work

This paper identifies the role of Br in determining the flow regime boundaries, and qualitatively explains the behaviour of flow transitions and the transition range. The complete quantitative correlations determining the flow regimes and their boundaries could not be obtained, since for a given microchannel geometry, the data is not available for the three flow regimes, to enable identification of the two boundaries. To obtain the quantitative transition flow range, the transitions must be obtained for the same geometry. The details of the energy and momentum transport processes in microchannels must also be theoretically investigated to better appreciate the role of Br in flow transitions.

4. Conclusions

1. In addition to the Reynolds number and the geometry of the microchannels, the Brinkman number has a role in determining the flow regime boundaries in microchannels.
2. The exponent, m, of Reynolds number in equation (2.1) determines the importance of the Reynolds number relative to the Brinkman number in determining the flow regime boundaries for a given microchannel geometry. Since $|m| > 1$, the Reynolds number has a higher role relative to the Brinkman number in determining the boundaries.
3. For the geometries studied, the laminar-to-transition boundary is approximately given by equation (5.1.),

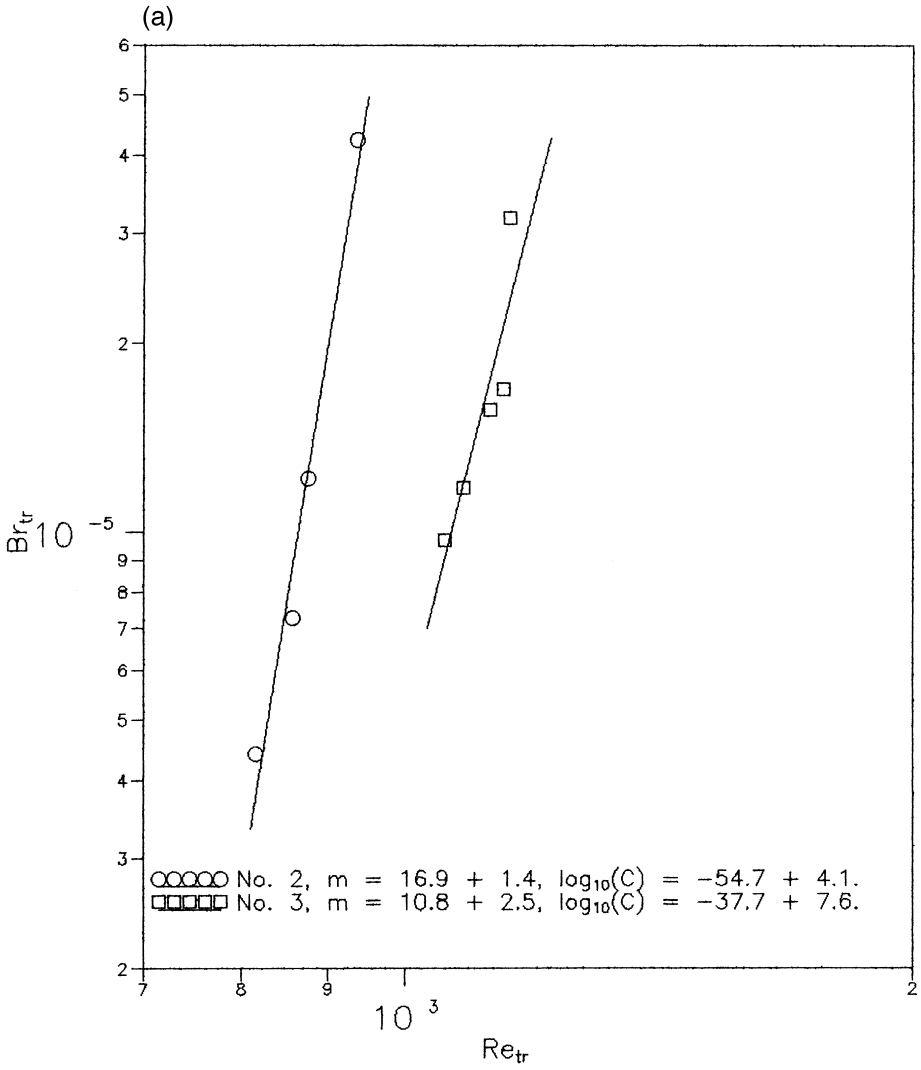

Fig. 4. (a) Locus of transition-to-turbulent flow points for test section nos 2 and 3; (b) locus of laminar-to-transition flow points for test section nos 5 and 6.

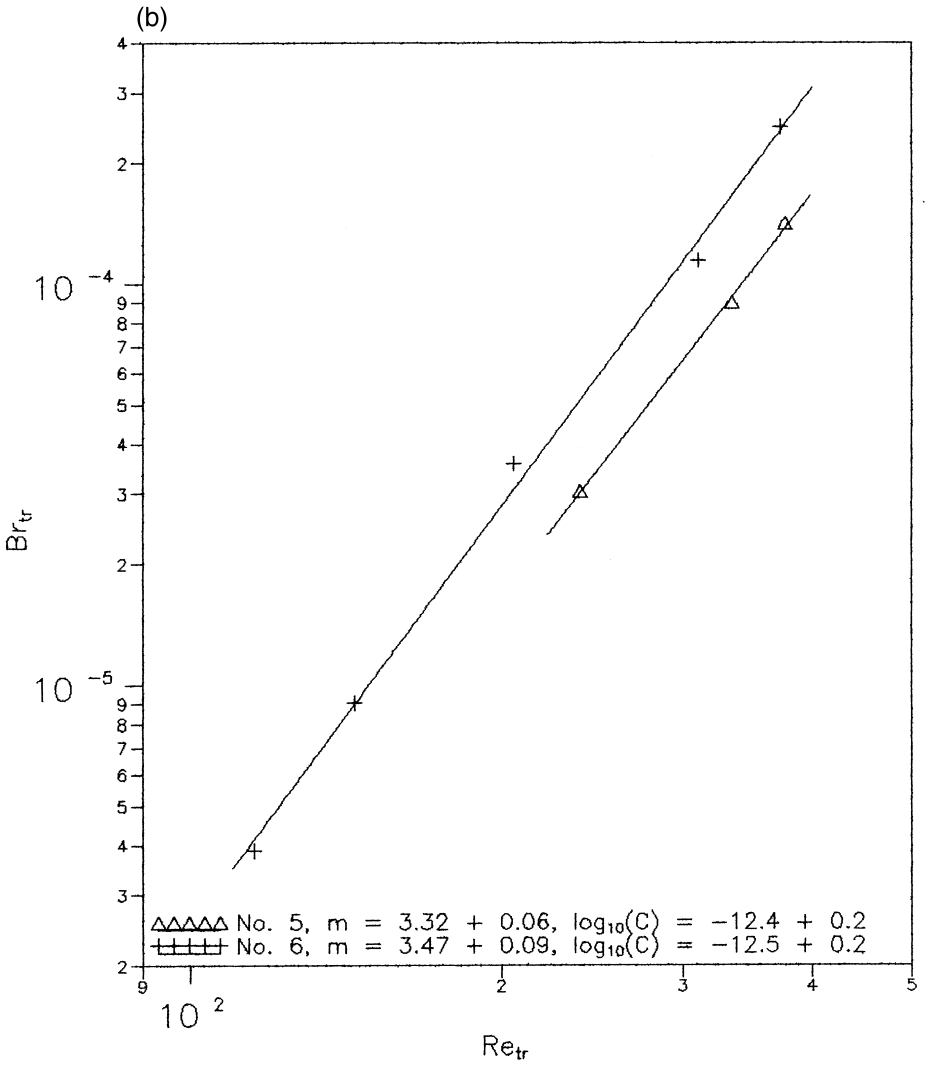

Fig. 4—*continued.*

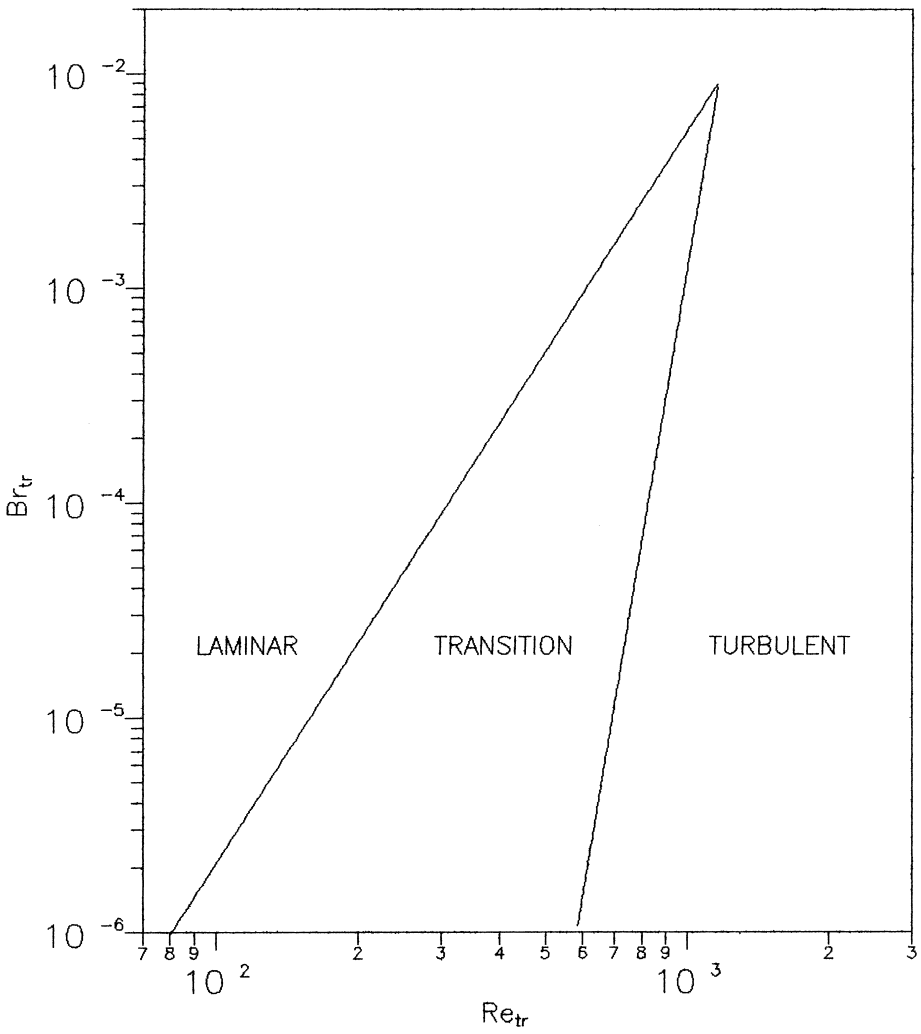

Fig. 5. Combined laminar-to-transition and transition-to-turbulent loci.

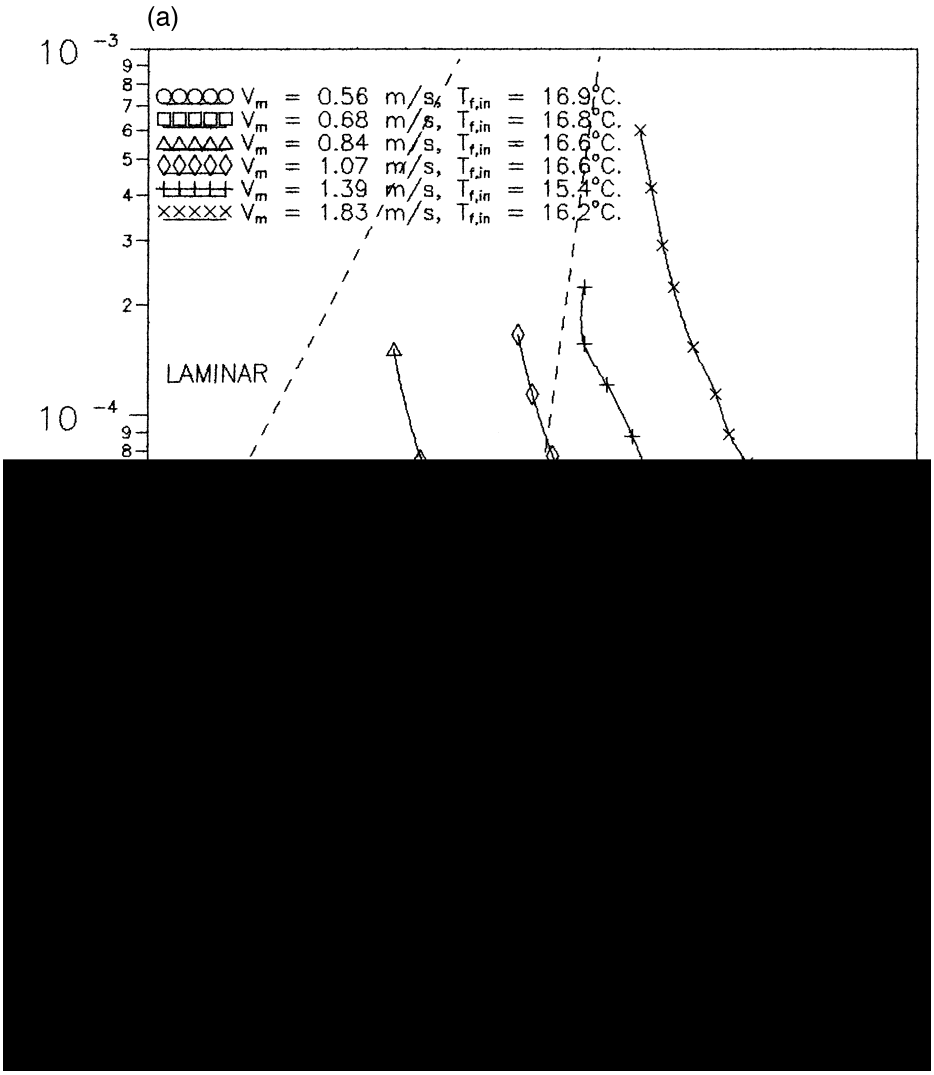
(a)
10^{-3}
9
8
7
6
5
4
3
2
10^{-4}
9
8
V_m = 0.56 m/s, $T_{f,in}$ = 16.9°C.
V_m = 0.68 m/s, $T_{f,in}$ = 16.8°C.
V_m = 0.84 m/s, $T_{f,in}$ = 16.6°C.
V_m = 1.07 m/s, $T_{f,in}$ = 16.6°C.
V_m = 1.39 m/s, $T_{f,in}$ = 15.4°C.
V_m = 1.83 m/s, $T_{f,in}$ = 16.2°C.
LAMINAR